Mesoscale modelling of laser powder-based directed energy deposition process

Available online at www.sciencedirect.com

ScienceDirect

Procedia CIRP 88 (2020) 393–398

www.elsevier.com/locate/procedia

13th CIRP Conference on Intelligent Computation in Manufacturing Engineering, CIRP ICME '19

Mesoscale modelling of laser powder-based directed energy deposition process

Gabriele Piscopo[a], Eleonora Atzeni[a], Alessandro Salmi[a,*], Luca Iuliano[a], Andrea Gatto[b], Giovanni Marchiandi[a], Andrea Balestrucci[c,a]

[a]*Politecnico di Torino, Department of Management and Production Engineering (DIGEP), Corso Duca degli Abruzzi 24, 10129 Torino, Italy*
[b]*Università degli Studi di Modena e Reggio Emilia, Department of Engineering "Enzo Ferrari" (DIEF), Via Vivarelli 10, 41125 Modena, Italy*
[c]*Istituto Italiano di Tecnologia, Center for Sustainable Future Technologies (CSFT@PoliTo), Via Livorno 60, 10144 Torino, Italy*

* Corresponding author. Tel.: +39-011-090.7263; fax: +39-011-090.7299. *E-mail address:* alessandro.salmi@polito.it

Abstract

Laser Powder-based Directed Energy Deposition (LP-DED) process is a cutting-edge Additive Manufacturing (AM) technology for metal part repair and production. The disruptive potentialities of LP-DED are nowadays limited by the difficulty in the identification of the optimized set of process parameters, typically obtained from long and expensive experimental trials. In this work, a thermal simulation tool able to predict material deposition behaviour is developed using a finite element code. An original method is defined to model the material addition and energy flow. The forecasting capabilities of the model in terms of penetration depth and track dimensions are evaluated by comparing the numerical outcomes with experimental data.

Peer review under the responsibility of the scientific committee of the 13th CIRP Conference on Intelligent Computation in Manufacturing Engineering, 17-19 July 2019, Gulf of Naples, Italy.

Keywords: Additive Manufacturing; Laser Powder-based Directed Energy Deposition (LP-DED); Al2024; Process simulation

1. Introduction

Additive Manufacturing (AM) processes are used in industry to produce prototypes and, nowadays, final components with complex shape [1]. Among the various AM technologies for metal part production, the Laser Powder-based Directed Energy Deposition process (LP-DED) is one of the most promising. The main advantages of LP-DED respect to other metal AM processes are the possibility to produce a component with large dimension (larger than one meter), the possibility to deposit material directly onto an existing surface and the possibility to produce functionally graded materials. The limited knowledge on the relations between the process parameters and the characteristics of the final product narrows today the use of LP-DED in the industry. Process parameters can be optimized using two different approaches: carrying out an experimental campaign or developing numerical predictive models [2,3]. Numerical models are widely used to investigate the temperature field, the residual stresses and the microstructure resulting from the building process. They allow identifying a stable process parameters window without realizing extensive and expensive experimental analyses.

The physical effects involved in the LP-DED process occur at different levels, from microscopic to macroscopic. For this reason, different modelling approaches are typically used in the simulation of AM processes. They differ in the characteristic dimension of the simulated phenomena and in the required output of the model. Fig. 1 illustrates the different simulation approaches available. Vasinonta *et al.* [4] used a two-dimensional thermo-mechanical model to simulate the production of a thin wall structure. In their model, only the conduction mechanism was considered, and the heat source was modelled as a point source. They identify two process maps for the evaluation of melt pool size and for the residual stresses. Hu and Kovacevic [5] developed a three-dimensional model in order to simulate the thermal behaviour of the melt pool during the deposition of a thin steel wall. They showed that the fusion depth and the average temperature in the

2212-8271
Peer review under the responsibility of the scientific committee of the 13th CIRP Conference on Intelligent Computation in Manufacturing Engineering, 17-19 July 2019, Gulf of Naples, Italy.
10.1016/j.procir.2020.05.068

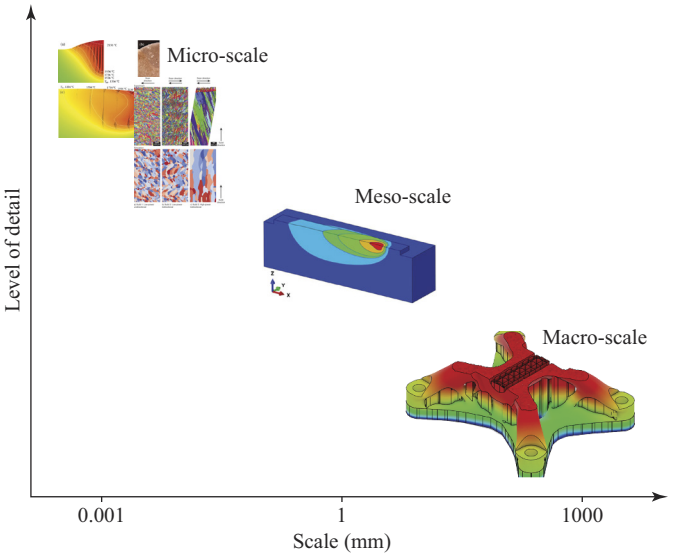

Fig. 1. Simulation approaches with different levels of detail and corresponding typical dimension.

processing zone can be regulated by varying the laser power at a constant traverse velocity. Toyserkani *et al.* [6] developed a three-dimensional model to study the effect of laser pulse shaping on the geometry of the deposited track. The model allows to predict the height of the track with an error lower than 15.5% and showed that layer height increases with laser pulse energy. Costa *et al.* [7], using a thermo-kinetic finite element model, investigated the effect of substrate dimension and idle time on the resulting microstructure of a ten-layer AISI 420 steel wall. They found that shorter idle time and smaller substrate size can reduce the proportion of tempered martensite and lead to a more uniform microstructure. Zekovic *et al.* [8] developed a thermo-mechanical model to study the effect of thermal cycle on residual stress distribution in a thin-walled structure. They showed that the distribution of residual stress depends on the deposition strategy and on the geometry of the component. Wang and Felicelli [9] developed a finite element model in order to predict the temperature distribution and the phase transformation that occur during the deposition of a thin wall of AISI 410 stainless steel. They showed that a more uniform microstructure is obtained using higher traverse speed. Long *et al.* [10] performed a thermo-mechanical simulation of the deposition of a thin wall of a nickel alloy. In this work, only the heat conduction was considered. They found that the stresses along the scan direction are predominant. Heigel *et al.* [11] developed a three-dimensional finite element model to simulate the effect of different convection mechanisms on residual stress produced during the deposition of thin-walled structure. They demonstrated that the use of a measurement-based convection model produces more accurate results.

In this work, a model to simulate the thermal phenomena that occur during the deposition of a single track of Al2024 aluminium alloy was developed. Abaqus/Standard 2017.HF8 was used to solve the thermal finite element model. The addition of material during the process has been modelled as a function of process parameters and has been implemented in the model using a specific subroutine. The temperature distribution obtained from the FE model has been used to estimate the penetration depth.

2. Governing equations

In the LP-DED process, a moving laser beam is focused onto a metal substrate and a melt pool is produced on its upper surface. A deposition head is used to feed the metal powder in the melt pool. When the powder material comes into the melt pool, it melts instantaneously, and a raised track is obtained. The powders are feed by the deposition head in the melt pool area by means of a shielding gas. This shielding gas causes a turbulent flow above the upper surface of the substrate, thus producing a forced convection mechanism. A simplified scheme of the process is illustrated in the Fig. 2.

The transient temperature distribution $T(x,y,z,t)$ in the model is governed by the general heat conduction equation

$$\rho c_p \frac{\partial T}{\partial t} = \frac{\partial}{\partial x}\left(k\frac{\partial T}{\partial x}\right)+\frac{\partial}{\partial y}\left(k\frac{\partial T}{\partial y}\right)+\frac{\partial}{\partial z}\left(k\frac{\partial T}{\partial z}\right)+Q \tag{1}$$

where ρ is the material density, c_p is the heat capacity, k is the thermal conductivity and Q is the internal heat source.

In order to consider the effects of the laser beam and of the convection mechanism, the general heat equation is subjected to the following boundary conditions:

$$-k(\nabla T\cdot\mathbf{n})\big|_{\Omega} = \begin{cases} I_L(x,y,z,t)-h_c(T-T_0)-\varepsilon_r\sigma\left(T^4-T_0^4\right) & \text{if } \Omega\in\Omega_L \\ -h_c(T-T_0)-\varepsilon_r\sigma\left(T^4-T_0^4\right) & \text{if } \Omega\notin\Omega_L \end{cases} \tag{2}$$

where Ω is the heat exchange surface, $\mathbf{n}$ is the normal vector to the surface Ω, Ω_L is the surface irradiated by the laser beam, $I_L(x,y,z,t)$ is the laser intensity distribution at the substrate, h_c is the heat convection coefficient, ε_r is the surface emissivity, and σ is the Stefan-Boltzmann constant.

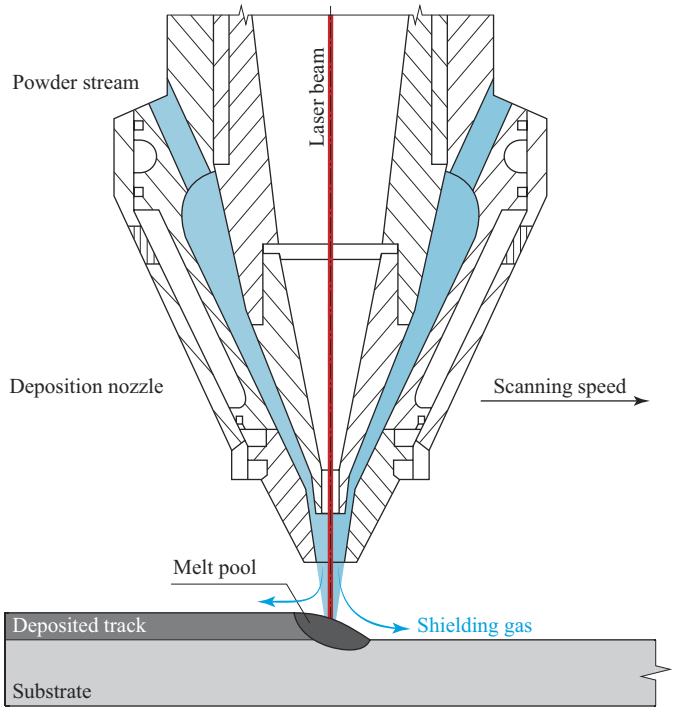

Fig. 2. Schematic illustration of the LP-DED process.

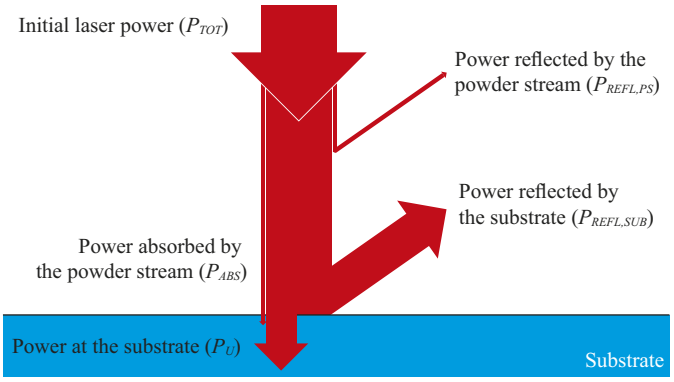

Fig. 3. Energy balance in the numerical model.

During the in-flight time, the metal powder interacts with the laser beam, and some of the initial laser power P_{TOT} is absorbed (P_{ABS}) or reflected/scattered by the metal powder stream ($P_{REFL,PS}$). These phenomena reduce the power available to create the melt pool and to increase the temperature of the powder during the in-flight distance. Moreover, reflection occurs at the substrate surface ($P_{REFL,SUB}$). Usually, the reduction of power is taken into account by means of a correction coefficient β that is used to calculate the useful power P_U available at the substrate using the equation

$$P_U = \beta \cdot P_{TOT} \tag{3}$$

Usually, the increase of powder temperature is included in thermal models by associating an initial temperature to the elements that simulate the track.

In this work a different strategy was adopted: due to the lack of experimental results on the temperature of the powder when deposited, the ambient temperature was initially associated to the track elements. Whereas the energy absorbed by the powder was included in the model by modifying the effective value of the heat source considering the energy balance. Specifically, the power fraction accounting for powder heating, P_{ABS}, was included in the effective power, and Eq. (3) changes to

$$P_E = P_U + P_{ABS} = P_{TOT} - \left(P_{REFL,PS} + P_{REFL,SUB}\right) = \varsigma \cdot P_{TOT} \tag{4}$$

where P_E is the effective power used to heat up and melt the powder and the substrate, and ς is the correction coefficient that takes into account only the power reflection mechanism

Table 1. Constant thermal properties of the Al2024 alloy.

Property	Value
Solidus temperature, T_{sol}	811 K
Liquidus temperature, T_{liq}	905 K
Latent heat, L	297 J/kg
Surface emissivity coefficient, ε_r	0.3

Table 2. Environmental properties.

Property	Value
Ambient temperature, T_0	293 K
Forced convection coefficient, $h_{c,for}$	100 W/(m²·K)
Natural convection coefficient, $h_{c,nat}$	9 W/(m²·K)

(Fig. 3). No data are available in the literature to split the distribution of power; for this reason, the ς coefficient was calibrated using experimental results.

The effective power is used to calculate the laser beam intensity as follow

$$I_L = \frac{P_E}{\pi r_L^2 h} \tag{5}$$

where I_L is the laser beam intensity, r_L is the laser beam radius at the substrate and h is the layer height.

3. Thermal FE model

In this work, the deposition of a single scan of Al2024 alloy on a substrate of the same material was simulated. Fig. 4 shows the temperature-dependent properties of the considered material according to Mills [12], whilst the constant thermal properties are detailed in Table 1. The phase transformation phenomena were considered in the model by including the latent heat of fusion and the non-equilibrium temperatures. The constant value of emissivity of the material was assumed from Romano *et al.* [13]. The effect of forced convection generated by the shielding gas was introduced in the model applying a convection coefficient on the upper surface of the substrate and on the deposited material. On the bottom surface of the substrate, natural convection was applied. Table 2 lists the values of the forced and natural convection coefficients, selected according to the work of Gouge *et al.* [14].

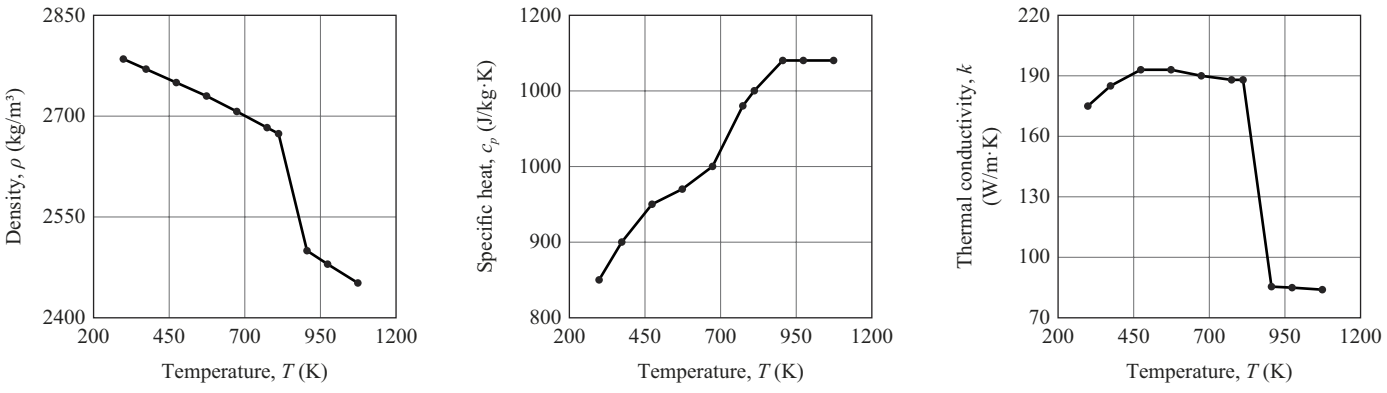

Fig. 4. Temperature dependent material properties of the Al2024 alloy.

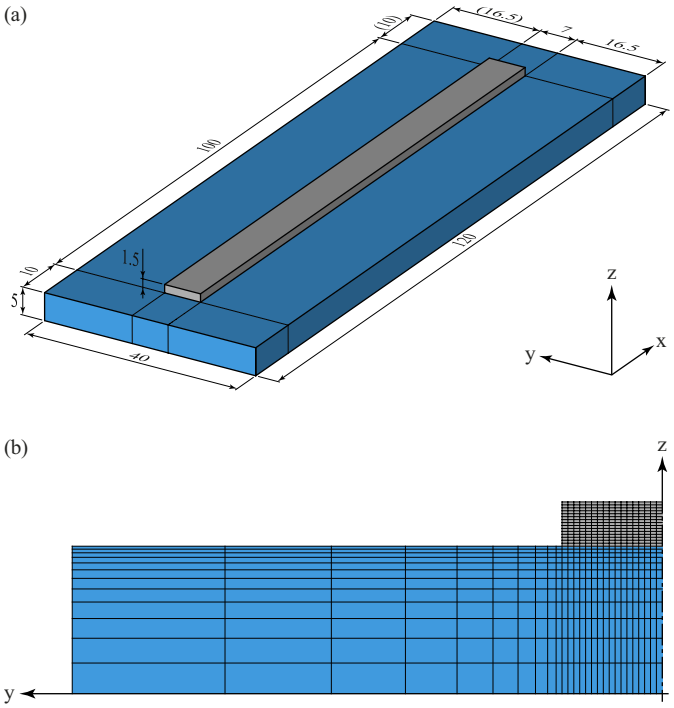

Fig. 5. (a) Geometry of the model; (b) Detail of the structured mesh.

3.1. Geometry and mesh

The geometry of the thermal model is shown in Fig. 5a. It consisted of two regions: the substrate (light blue) and the activation volume (grey). The activation volume is a thin layer that represents the volume of elements that could be potentially activated during the generation of the track. However, the effective dimensions of the activated (i.e. deposited) volume will finally depend on process parameters, as detailed in the next section. The substrate was 40 mm wide, 120 mm long and 5 mm thick. On the substrate, the activation volume with a width of 7 mm, a height of 1.5 mm and a length of 100 mm was modelled. A structured mesh was used as represented in n Fig. 5b with 8-node linear elements. In the activation volume, dimensions of the elements were 0.2 mm wide, 0.2 mm long and 0.1 mm height. In the substrate, a coarser mesh was used, and the maximum element dimension was 5.2 mm along the width and 1 mm along the depth.

3.2. Activation strategy

The progressive addition of material that occurs during the process is implemented by adding elements into the computational domain. The elements that will be included are selected customizing the UEPACTIVATIONVOL user subroutine in order to define the activation strategy (Fig. 6). This subroutine allows adding elements into the computational domain continuously, solving equations defined by the user. The strategy adopted in this model consists of an algorithm that, following the laser path, activates those elements that are included in the activated volume defined by experimental regression formulas. Specifically, the layer width, W, and the layer height, H, are expressed as a function of laser power (P) and scanning speed (v_s), according to Caiazzo *et al.* [15]

$$W = 4.7 + 1.4 \cdot P - 7 \cdot 10^{-3} \cdot v_s \quad (6)$$

$$H = 2.1 - 0.2 \cdot P - 10^{-3} \cdot v_s \quad (7)$$

These equations define the dimensions of the track in the cross section for a constant powder feed rate, $Q = 3$ g/min. The third dimension, along the scanning direction, is assumed to be equal to the beam diameter. An element is activated if more than half of its nodes are enclosed in the activated volume.

4. Results and discussion

In the following paragraphs, the results of the FE model are presented. Experimental data from two works [15,16] were used for model calibration and validation, respectively.

4.1. Model calibration

The calibration of the model was performed by varying the value of the ς correction coefficient and comparing the penetration depth obtained from numerical results with experimental results from Caiazzo *et al.* [15]. The initial value of the correction coefficient was set to 0.5 and it converged to the value of 0.4. Fig. 7 shows the comparison of melt pool dimensions between experimental and numerical results, from the calibrated model. Especially, the process parameters were $P = 2$ kW and $v_s = 300$ mm/min.

4.2. Model validation

The validation of the model was performed on a second set of experimental data from Caiazzo and Caggiano [16]. In order to evaluate the effect of process parameters on the geometry of the deposited track, a factor that combines laser power, scanning speed, and beam diameter was considered [17]. This

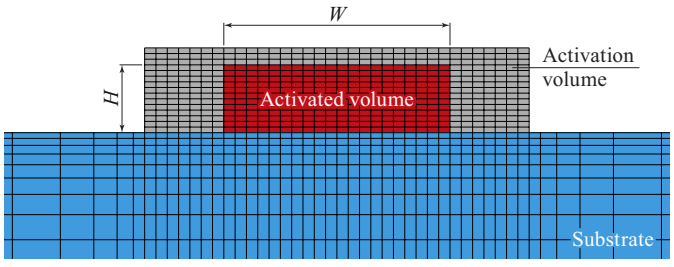

Fig. 6. Activation volume and activated elements.

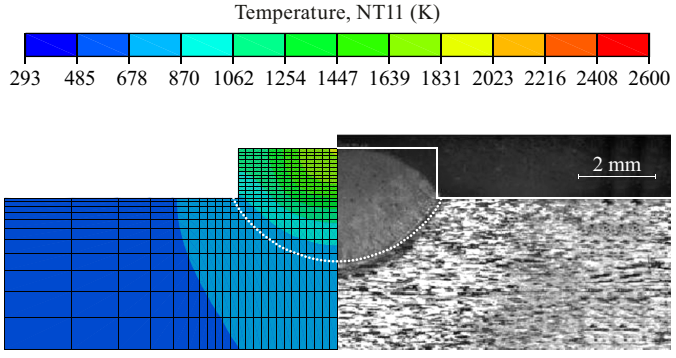

Fig. 7. Experimental and numerical results after model calibration.

Table 3. Sets of process parameters used to validate the model.

	Set #1	Set #2	Set #3
Laser power, P (kW)	2	3	3
Scanning speed, v_s (mm/min)	500	500	300
Mass feed rate, Q (g/min)	3	3	3
Specific energy, E_s (J/mm^3)	40	60	100

factor is the specific energy, E_s, and it is defined as

$$E_s = \frac{P}{2 v_s r_L} \tag{8}$$

From a technological point of view, the specific energy represents the amount of thermal energy introduced in the system per unit area. From experimental data in [16], three sets were extracted, with the same mass feed rate $Q = 3$ g/min but increasing values of specific energy. Table 3 summarizes the process parameters used for the validation of the model.

Fig. 8 shows the numerical and the experimental dimensions W and H as a function of the specific energy. Comparing the results, it is possible to observe that the prediction error of the model is very low, about 3% and 8% respectively for W and H, with corresponding maximum deviations of 0.20 mm and 0.13 mm. It is possible to observe that similar values of height were obtained for the three sets. This means that the effect of a specific energy increase on H is negligible for the considered range. In other words, these results suggest that the specific thermal energy is not the main responsible for the height change of the deposited track. On the contrary, a significant influence of the specific energy on the track width, W, was observed. Doubling the specific energy leads to an increase of W by around 50%.

The coloured maps in Fig. 9 show the temperature distributions in the cross section (XZ plane) for the three sets. The iso-temperature curves have a semi-elliptical shape symmetric with respect to the laser beam axis, as characteristic for the LP-DED process. The iso-temperature curve

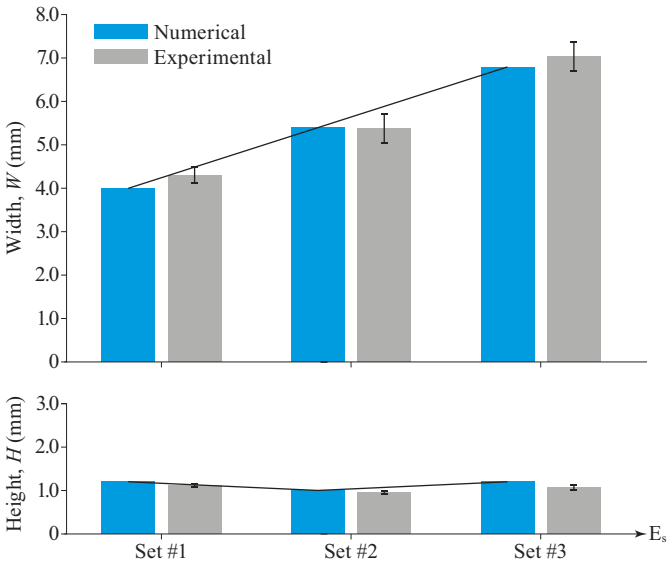

Fig. 8. Numerical and experimental dimensions of the track cross section as a function of the specific energy.

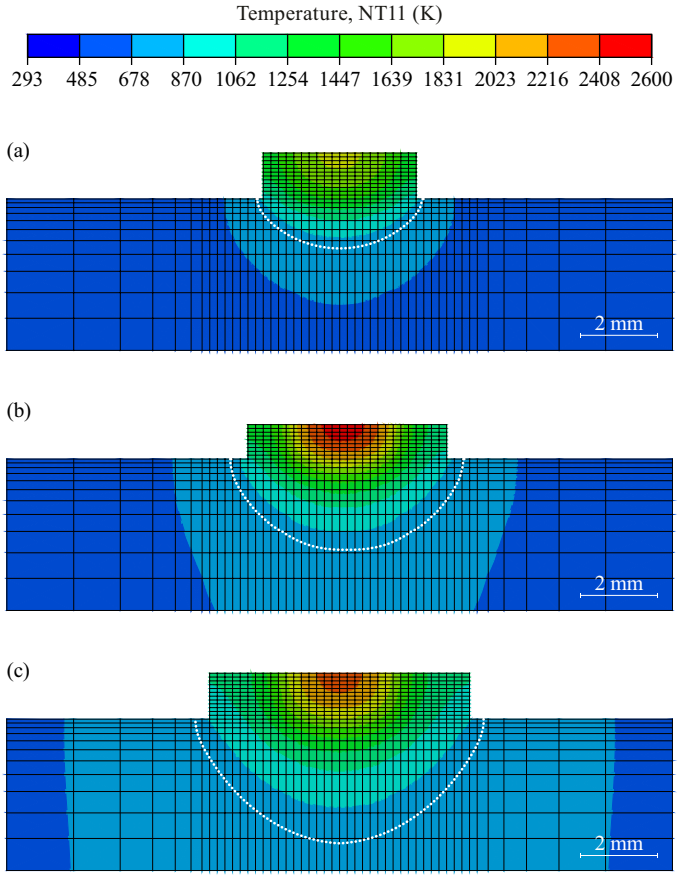

Fig. 9. Numerical temperature distributions for (a) Set #1, (b) Set #2 and (c) Set #3. The dotted line represents the melt pool boundary.

corresponding to the solidus temperature is used to evaluate the boundary of the melt pool. The penetration depth was calculated considering the distance along the building direction, Z axis, from the lowest point of this boundary curve to the substrate top surface.

The penetration depths are shown in Fig. 10 as a function of the specific energy. Experimental values are also included in the same graph for comparison. On average, the numerical model slightly overestimates the penetration depth, and the deviation ranges from –0.19 mm to 0.08 mm. Hence, the model is found to be able to predict the penetration depth with a mean error of about 5%, limited to the experimental range considered for the validation. It is possible to observe that increasing the

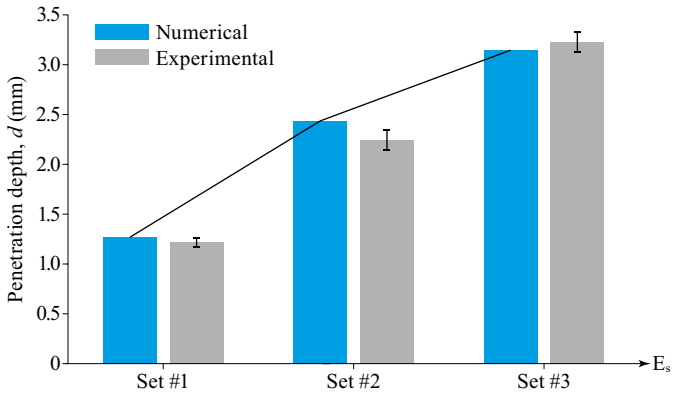

Fig. 10. Numerical and experimental values of the penetration depth as a function of the specific energy.

value of the specific energy, higher values of penetration depth were obtained. As clearly shown by results, the specific energy highly influences the melt pool width and the penetration into the substrate. By increasing the laser power (Set #2 vs Set #1), higher energy is transferred to the substrate; by decreasing the scanning speed (Set #3 vs Set #2), the heat has time to be transferred by conduction through the material.

It is worth to note that the observed prediction errors of the numerical model are affected by the simplifying assumptions of the model. Specifically, the minimum mesh size is set to 0.1 mm in height and 0.2 mm in width. Moreover, some phenomena related to the physics of the process are neglected, as, for instance, the Marangoni flow, the powder flow distribution, and the geometrical interaction between the laser and the melt-pool.

5. Conclusions

In this paper, a novel framework for the thermal simulation of Laser Powder-based Directed Energy Deposition (LP-DED) process was developed. A mesoscale approach was used in order to investigate the effect of process parameters on a single track of Al2024 aluminium alloy deposited on a substrate of the same material. The activation strategy used to simulate the addition of material during the process is based on analytical relationships obtained from regression analysis and this allows to define the volume of elements added into the computational domain. This volume depends on the process parameters: laser power and scanning speed. The model allowed to predict the geometry of the deposited material with an error lower than 8%. The temperature distribution obtained from the model was used to estimate the penetration depth. The comparison between the numerical and the experimental values of penetration depth showed a good agreement.

Acknowledgements

This research was partially supported by the STAMP – Sviluppo Tecnologico dell'Additive Manufacturing in Piemonte project founded by Piemonte Region (Italy) in the framework of POR-FESR, 2014-2020.

References

[1] Gu D, Meiners W, Wissenbach K, Poprawe R. Laser additive manufacturing of metallic components: materials, processes and mechanisms. International materials reviews. 2012;57:133-64.
[2] Piscopo G, Atzeni E, Salmi A. A Hybrid Modeling of the Physics-Driven Evolution of Material Addition and Track Generation in Laser Powder Directed Energy Deposition. Materials. 2019;12.
[3] Piscopo G, Salmi A, Atzeni E, Iuliano L, Busatto M, Tusacciu S, Lai M, Biamino S, Toushekhah M, Saboori A, Fino P. On the Effect of Deposition Patterns on the Residual Stress, Roughness and Microstructure of AISI 316L Samples Produced by Directed Energy Deposition. Progress in Digital and Physical Manufacturing. 2020. p. 206-12.
[4] Vasinonta A, Beuth JL, Griffith ML. Process maps for controlling residual stress and melt pool size in laser-based SFF processes. Solid freeform fabrication proceedings: Proc. 2000 Solid Freeform Fabrication Symposium, Austin; 2000. p. 206.
[5] Hu D, Kovacevic R. Modelling and measuring the thermal behaviour of the molten pool in closed-loop controlled laser-based additive manufacturing. Proceedings of the Institution of Mechanical Engineers, Part B: Journal of Engineering Manufacture. 2003;217:441-52.
[6] Toyserkani E, Khajepour A, Corbin SJO, engineering li. 3-D finite element modeling of laser cladding by powder injection: effects of laser pulse shaping on the process. 2004;41:849-67.
[7] Costa L, Vilar R, Reti T, Deus A. Rapid tooling by laser powder deposition: process simulation using finite element analysis. Acta Materialia. 2005;53:3987-99.
[8] Zekovic S, Dwivedi R, Kovacevic R. Thermo-structural finite element analysis of direct laser metal deposited thin-walled structures. Proceedings SFF Symposium, Austin, TX2005.
[9] Wang L, Felicelli S. Process modeling in laser deposition of multilayer SS410 steel. Journal of Manufacturing Science and Engineering. 2007;129:1028-34.
[10] Long R-S, Liu W-J, Fei X, Wang H-B. Numerical simulation of thermal behavior during laser metal deposition shaping. Transactions of nonferrous metals society of china. 2008;18:691-9.
[11] Heigel J, Michaleris P, Reutzel E. Thermo-mechanical model development and validation of directed energy deposition additive manufacturing of Ti–6Al–4V. Additive manufacturing. 2015;5:9-19.
[12] Mills KC. Recommended values of thermophysical properties for selected commercial alloys: Woodhead Publishing; 2002.
[13] Romano J, Ladani L, Sadowski M. Thermal modeling of laser based additive manufacturing processes within common materials. Procedia Manufacturing. 2015;1:238-50.
[14] Gouge MF, Heigel JC, Michaleris P, Palmer TA. Modeling forced convection in the thermal simulation of laser cladding processes. The International Journal of Advanced Manufacturing Technology. 2015;79:307-20.
[15] Caiazzo F, Alfieri V, Argenio P, Sergi V. Additive manufacturing by means of laser-aided directed metal deposition of 2024 aluminium powder: Investigation and optimization. Advances in Mechanical Engineering. 2017;9:1687814017714982.
[16] Caiazzo F, Caggiano A. Laser direct metal deposition of 2024 Al alloy: Trace geometry prediction via machine learning. Materials. 2018;11:444.
[17] Toyserkani E, Khajepour A, Corbin SF. Laser cladding: CRC press; 2004.